Mon. Not. R. Astron. Soc. **000**, 1–14 (2016) Printed 8 June 2016 (MN LATEX style file v2.2)

NIR Tully-Fisher in the Zone of Avoidance. – III. Deep NIR catalog of the HIZOA galaxies

Khaled Said[1,2,3⋆], Renée C. Kraan-Korteweg[1], T. H. Jarrett[1], Lister Staveley-Smith[2,3], and Wendy L. Williams[4]

[1]*Astrophysics, Cosmology and Gravity Centre (ACGC), Astronomy Department, University of Cape Town, Private Bag X3, Rondebosch, 7701, South Africa*
[2]*International Centre for Radio Astronomy Research (ICRAR), M468, The University of Western Australia, 35 Stirling Highway, Crawley, WA 6009, Australia*
[3]*ARC Centre of Excellence for All-sky Astrophysics (CAASTRO)*
[4]*School of Physics, Astronomy and Mathematics, University of Hertfordshire, College Lane, Hatfield AL10 9AB, UK*

Accepted 00. Received 00; in original form 00

ABSTRACT

We present a deep near-infrared catalog of the Parkes H I Zone of Avoidance (HIZOA) survey, which forms the basis of the investigation of matter distribution in the Zone of Avoidance. Observations were conducted between 2006 and 2013 using the Infrared Survey Facility (IRSF) installed on the 1.4 m telescope situated at the South African Astronomical Observatory site in Sutherland. The survey covers all HIZOA detection in 1124 fields, and yields 915 galaxies. An additional 105 2MASS fields in the southern ZOA but not in the HIZOA survey were observed, resulting in 129 galaxies. The average K_s band seeing and sky background for the survey are 1.38 arcsec and 20.1 mag, respectively. The detection rate as a function of stellar density and dust extinction is found to mainly depend on the H I mass of the H I detected galaxy. We found 285 galaxies in the NIR catalog to have 2MASS counterparts and 30 galaxies to have UKIDSS Galactic Plane Survey (GPS) counterparts. The K_s band K_{s20} fiducial elliptical aperture magnitude derived in this paper agrees, within the uncertainty, with the same parameter reported in the 2MASX catalog. Small deviation (< 0.8 mag) for both faint galaxies (> 14 mag) and bright galaxies (< 9 mag) are explained by the difference of the pixel scale of the IRSF and 2MASX instruments. A modified version of our photometry pipeline was used to derive the UKIDSS photometric parameters of the UKIDSS counterparts for comparison purposes. Good agreement was also found with the K_s band K_{s20} fiducial elliptical aperture magnitude derived from the UKIDSS GPS data. These comparisons show the robustness of the isophotal results. The agreement of IRSF with the UKIDSS GPS, which is one magnitude deeper, proves that IRSF imaging is not suffering from foreground contamination ,after star removal, nor is it adversely under-estimating the isophotal flux of the ZoA galaxies.

Key words:

1 INTRODUCTION

The Milky Way obscures the background extragalactic sky through dust extinction, notably within ± 5 degrees of the Galactic Plane, and stellar confusion. This results in the so-called "Zone of Avoidance" (ZOA), literally meaning that the region is devoid of galaxies, and accordingly, extragalactic astronomers avoid working in this region of the sky. This has led to a gap in our understanding of Large Scale Structure (LSS) in the ZOA, especially the conspicuous features that cross the ZOA, such as the Perseus-Pisces Supercluster (PPS; Einasto et al. 1980; Giovanelli & Haynes 1982; Focardi et al. 1984; Hauschildt 1987), the Great Attractor (GA; Dressler et al. 1987; Lynden-Bell et al. 1988; Woudt et al. 1999) and the Local Void (LV; Tully & Fisher 1987; Kraan-Korteweg et al. 2008).

Galaxy peculiar velocities, deviations from the isotropic Hubble expansion, are sensitive to LSS such as GA (Dressler et al. 1987) and can be used alongside redshift surveys for cosmography and to study the dynamics of the Local Group (LG), cosmic flow fields, and the origin of the observed dipole in the Cosmic Microwave Background (CMB) (e.g. Masters et al. 2006; Springob et al. 2007; Masters et al. 2008; Magoulas et al. 2012; Courtois et al. 2013; Mutabazi et al. 2014; Hong et al. 2014; Springob et al. 2014; Tully et al. 2014; Carrick et al. 2015; Springob et al. 2016; Tully et al. 2016). The use of infrared wavelengths in these studies (Masters et al. 2008; Sorce et al. 2013, 2014; Neill et al. 2014; La-

⋆ E-mail: khaled@ast.uct.ac.za

gattuta et al. 2013) has minimized the ZOA, but the most obscured part of the ZOA ($|b| \leqslant 5^\circ$) remains problematic.

This project aims to derive the peculiar velocities of galaxies in the ZOA to supplement the above studies and provide a truly all sky peculiar velocity survey. In this series of papers, we aim to map most of the dynamically important structures in the ZOA such as PPS, GA and LV, in greater detail.

The requirements for such a survey are: (i) A calibrated and unbiased TF relation to be used as the global template relation; (ii) 21 cm observations of spiral galaxies in the ZOA to extract the redshift and the rotational velocity of galaxies from; (iii) follow-up NIR imaging survey of the H I survey to measure the apparent magnitude of each galaxy. Once we have these three ingredients, the absolute magnitude can be measured from the template relation given the rotational velocity. The distance to each galaxy can then be calculated independent of the redshift using the distance modulus.

In Said et al. (2015) the TF template is constructed using isophotal magnitude of 888 spiral galaxies. The advantage of using isophotal and not total magnitude is twofold: First, it is more robust and can easily measured in and out of the ZOA. Second, it shows consistency through different surveys which means it can be used to combine data from different survey without corrections (see, Fig. 1 in Said et al. 2015). A correction model for the change in the shape of galaxies due to dust extinction is also presented in Said et al. (2015).

Said et al. (2016) presents the second element for this survey which are the 21 cm H I-line spectra of inclined, $(b/a)^\circ < 0.5$, spiral galaxies. The average signal-to-noise ratio for this H I survey was 14.7 which is adequate for TF studies. Five different types of line-width are also discussed to select the most robust one. Conversions between these widths also derived to allow combination of data from different surveys.

This paper is dedicated to a systematic NIR follow-up observations of all galaxies in the HIZOA catalog (Donley et al. 2005; Kraan-Korteweg et al. 2008; Staveley-Smith et al. 2016). At low Galactic latitude NIR wavelengths should be used instead of optical wavelength because of the ability of NIR radiation to penetrate through dust (Kraan-Korteweg & Lahav 2000; Kraan-Korteweg 2005). In the last few decades many surveys have used the NIR to unveil the LSS hidden behind the Milky Way.

The 2MASS extended source catalog (2MASX) contains galaxies that never been seen before in the ZOA (Jarrett et al. 2000). Jarrett et al. (2000) present new extended sources in the ZOA at Galactic longitude between 40° and 70°.

Deeper NIR surveys are used specifically for surveys in the ZOA. Nagayama et al. (2004) used the same instrument used in this paper to conduct a NIR survey around the radio galaxy PKS1343-601. They detect 19 galaxies and another 38 as galaxy candidates and only three of these galaxies were known previously. Woudt et al. (2005) also used the IRSF telescope to obtain deep photometry for 76 galaxies used in the determination of a distance to Norma cluster. Nagayama et al. (2006) used a deep NIR survey of a luminous cluster in the GA region and identified 111 galaxy candidates. Longer wavelengths are also used in the ZOA. Jarrett et al. (2007) used mid-infrared wavelengths to unveil two galaxies in the GA region. A Large deep NIR survey of the Norma Wall (NWS: Riad et al. 2010; Riad 2010; Kraan-Korteweg et al. 2011; Riad et al,. in prep) was also conducted on the IRSF telescope. This survey resulted in a catalog of 4360 galaxies with a completeness limit of 15.6, 15.3 and 14.8 mag in the J, H, and K_s bands, respectively. Given the success of these surveys, we started a follow-up NIR survey of the HIZOA galaxies in the southern ZOA.

This paper is organized as follow. Section 2 discuss the observations, calibration and observatory site conditions. In Section 3 we discuss the identification, star subtraction and the photometry pipe-line. The final extended source catalog and parameter characterization are presented in Section 4. Completeness as a function of dust extinction and stellar density is discussed in detail in Section 5. Comparison of the resulting photometry the 2MASS and UKIDSS surveys is presented for quantification in Section 6. We summarise our results in Section 7. All magnitudes are quoted in the Vega System.

2 OBSERVATIONS

Deep NIR follow-up observations of all HIZOA-galaxies were conducted with the Infrared Survey Facility (IRSF) installed on the 1.4 m telescope situated at the South African Astronomical Observatory (SAAO) site in Sutherland, South Africa. The Simultaneous 3-colour (J, H, and K_s) Infrared Imager for Unbiased Survey (SIRIUS; Nagayama et al. 2003) camera on the IRSF has a field of view of 7.7×7.7 arcmin^2 (ideally suited for HIZOA follow-up given the 4 arcmin positional accuracy of the H I detection) with a resolution of 0.45 arcsec pixel^{-1} compared to 2.0 arcsec pixel^{-1} in 2MASS (Skrutskie et al. 2006). A pilot project and the first results of the catalog were published in Williams et al. (2014). Photometry for 557 galaxies in the HIZOA catalog with $cz \leqslant 6000$ km s^{-1} were also presented. For completion we included the 578 fields presented in Williams et al. (2014) in the current study.

An additional 105 2MASX fields in the southern ZOA but not in the HIZOA survey were also observed. The H I spectral line data for these 105 2MASX fields are from Parkes observations and available either from the 2MASS Tully-Fisher Survey (Hong et al. 2013) or from (Said et al., in prep.). These additional galaxies are bright ($K_s^\circ = 11.25$ mag) 2MASX edge-on ($b/a = 0.5$) selected galaxies in the southern ZOA ($5^\circ \leqslant |b| \leqslant 10^\circ$).

2.1 Data acquisition

Data acquisition started in 2006 and finished in 2013, resulting in a complete deep NIR survey of all the HIZOA targets. The targeted survey images have exposure times of 10 min, which result in a 2 mag deeper survey compared to 2MASX in the K_s-band. We used the dithering technique to overcome the problem of faulty pixels in the NIR detector. We repeated a 24 second exposure 25 times with a dithering step of 15 arcsec. This dithering resulted in increasing the final image size to 8.6×8.6 arcmin^2. A total of 12 weeks were allocated to this project starting in 2009. 101 fields were observed between 2006 and 2008 as part of other projects. Table 1 shows the observations, number of allocated weeks, number of fields observed and the Observer In Charge (OIC). Substantial time was lost during the 2009 and 2010 runs due to bad weather and cooling system problems.

2.2 Data reduction and calibration

The primary data reduction, including dark frame subtraction, flat field correction, sky subtraction, dither combine and astrometric

Table 1. IRSF observations and the Observer In Charge (OIC). OIC: Wendy Williams (WW), Tom Mutabazi (TM) and Khaled Said (KS).

Year	Month(s)	Allocated weeks	No. of fields	OIC
2006-2008			101	
2009	March/April	2	249	WW
2009	March/April	2	67	WW
2010	June/July	3	138	WW
2012	May	2	231	TM
2013	April	3	430	KS

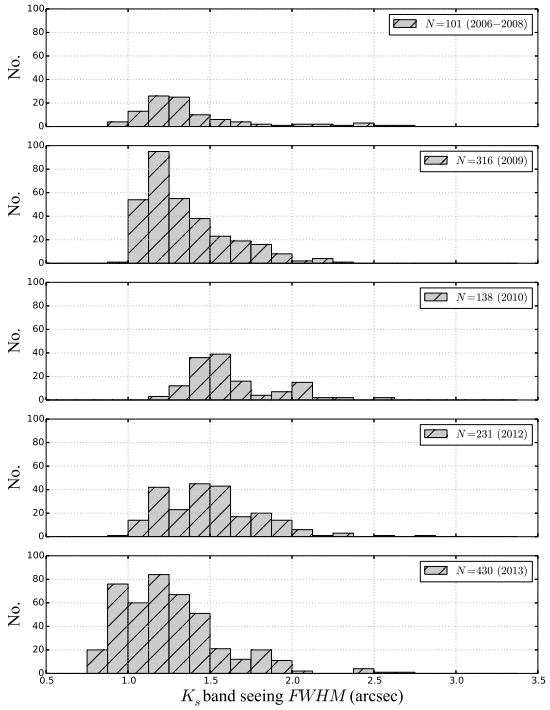

Figure 1. Distribution of K_s band measured image seeing *FWHM* from 2006 to 2013.

and photometric calibration, was carried out using the pipeline software for SIRIUS[1].

2.3 Observatory site conditions and quality control

Figures 1 and 2 show the distribution of the K_s band seeing and the deviation of magnitude zero point from the mean for 1229 observed fields, respectively, as a function of observation date.

An average K_s band seeing of 1.38 arcsec and an average K_s band magnitude zero point of 20.1 mag were found for the whole survey. These values agree with those found in the NWS (Riad 2010; Kraan-Korteweg et al. 2011). Figure 1 shows that 95% of the survey has a seeing < 2.0 arcsec. Figure 2 shows that 85% of the survey deviates from the mean magnitude zero point by $\pm$ 0.2 mag. However the deviations of magnitude zero point from the mean are not significant, Fig. 2 shows a clear trend with time which means that the sky is getting brighter with time. All fields with either seeing or zero point magnitude outside of these two ranges were inspected visually one-by-one to check for image quality. Poor quality fields were re-observed under photometric conditions[2].

[1] http://irsf-software.appspot.com/yas/nakajima/sirius.html

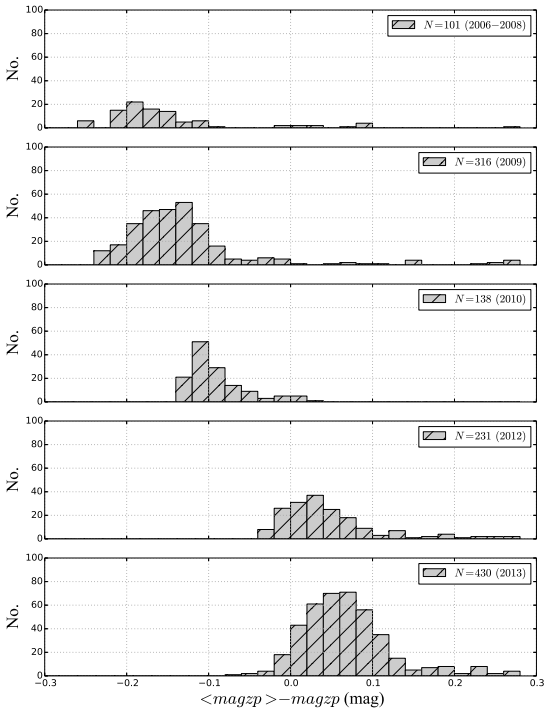

Figure 2. Distribution of K_s band photometric zero point magnitude from 2006 to 2013.

Figure 3 shows one field that was re-observed, where the left panel field observed under non-photometric conditions and re-observed under photometric conditions on the right. The field on the left hand side was observed under partially cloudy sky which affects both the seeing and magnitude zero point. The K_s band seeing for the left hand side field is 2.6 arcsec. The K_s band zero point magnitude for the field on the left hand side was found to be 18.1 mag. In contrast, the right hand side field was observed under photometric conditions. The K_s band seeing and zero point magnitude for the right hand side field are 0.9 arcsec and 20.1 mag, respectively.

The counterpart of the HIZOA galaxy J1624-45A is an edge-on galaxy and is marked with the white ellipse on the left-bottom corner of each field. It demonstrates how important photometric conditions are for these kind of surveys. The extent of the galaxy on the left hand side is underestimated while the real size of the galaxy is shown on the right hand panel.

3 EXTENDED SOURCE IDENTIFICATION AND REDUCTION

Procedures for source identification, star subtraction and photometry are described in detail in Williams et al. (2014). In this section we will therefore only summarize the most important aspects.

The three J, H, and K_s bands are combined in the standard

[2] These fields are removed and replaced with the ones observed under photometric conditions from the final catalog but we made both FITS files available for comparison purpose

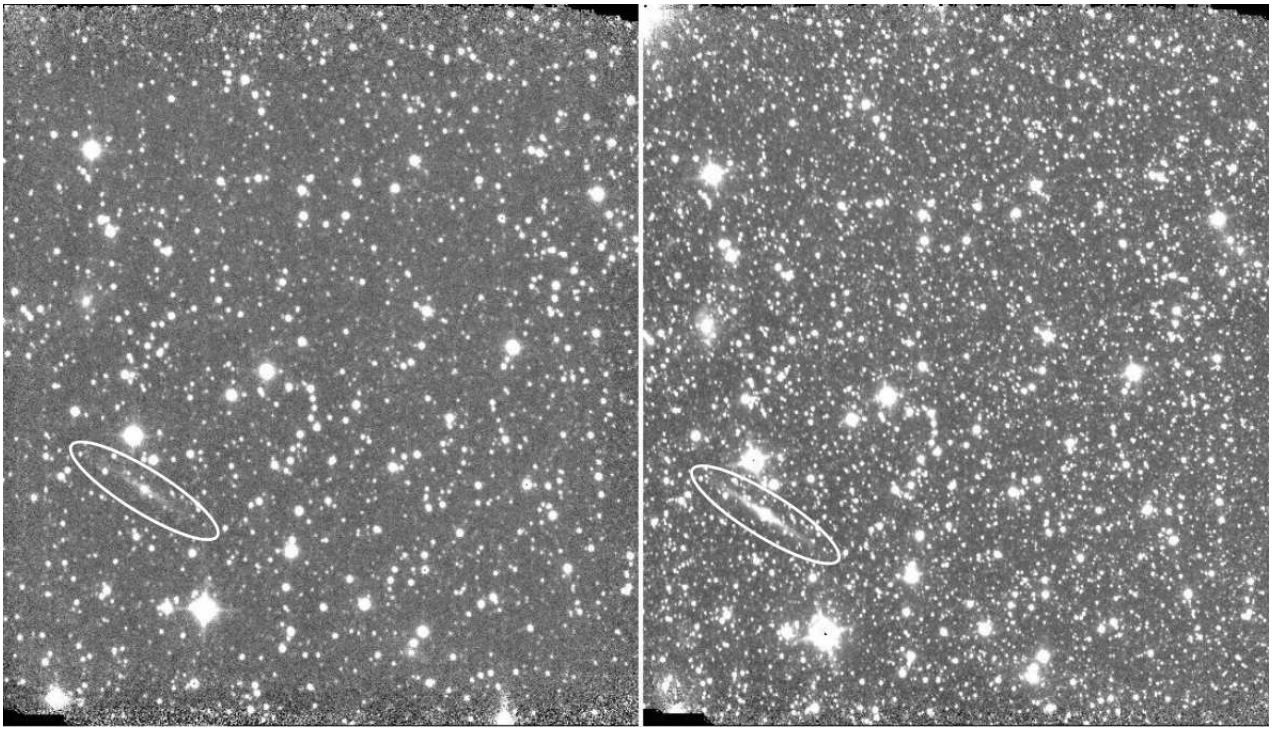

Figure 3. K_s band photometric vs non-photometric fields. Both fields are 8.6×8.6 arcmin; the field on the left was observed under non-photometric conditions while the field on the right was re-observed under photometric conditions. The K_s band seeing and zero point magnitude for the left hand side field are 2.6 arcsec and 18.1 mag, respectively, while the K_s band seeing and zero point magnitude for the right hand side field are 0.9 arcsec and 20.1 mag, respectively.

fashion; blue J band, green H band, and red K_s band, to create RGB image of each field. These three color images were inspected by eye, one-by-one, to check for galaxies in it. The detected galaxies in each field were then compared with the H I spectrum from the HIZOA survey to identified the counterpart.

In the ZOA, stellar density is very high and star subtraction is used ahead of photometric measurement. Poor star subtraction may lead to contaminating the galaxy flux with foreground stars. The method for star subtraction by fitting the point spread function (PSF) was used for the whole survey. We refer the reader to Williams et al. (2014) which provides a description of the processes of star subtraction and photometry.

4 FINAL EXTENDED SOURCE CATALOG

The final extended source catalog contains 1044 galaxies extracted from 1229 fields observed in J, H, and K_s bands. The catalog and FITS files for the three bands J, H, and K_s are available electronically. An example of the catalog is given here for the brightest 100 galaxies in the catalog.

4.1 NIR Parametrization and catalog

The main goal of this paper is to provide accurate NIR photometric parameters for galaxies hidden behind the ZOA. These parameters will be used in the forthcoming NIR TF analysis. In this section we provide the required parameters for the TF analysis. For consistency with Williams et al. (2014), we employ the same algorithm to the whole survey which uses the same methods and naming described in Cutri et al. (2003). Table 2 and Figure 4 present the photometry and stamps of the brightest 100 galaxies in the catalog in order of isophotal K_{s20} fiducial elliptical aperture magnitude, respectively. The catalog presented in its entire form online. The NIR parameters listed in the catalog are as follows:

Column (1) - unique ZOA ID formed from sexigesimal coordinates [ZOAhhmmss.sss±ddmmss.ss] as reported in Williams et al. (2014).

Column (2) - HIZOA ID as reported in the HIZOA survey publications (Donley et al. 2005; Staveley-Smith et al., 2015; Kraan-Korteweg et al., in prep.)[3].

Columns (3) - Survey name.

Columns (4 and 5) - Right Ascension (RA) and Declination (Dec.) in the J2000.0 epoch.

Columns (6 and 7) - Galactic coordinates [degree].

Columns (8) - J-band ellipticity ($\epsilon = 1 - b/a$) and associated error.

Columns (9) - Isophotal K_{s20} fiducial elliptical aperture semi-major axis [arcsec].

Columns (10-12) - J, H, and K_s bands K_{s20} fiducial elliptical aperture magnitudes and associated errors [mag].

Columns (13-15) - J, H, and K_s bands central surface brightness [mag arcsec^{-2}].

Columns (16) - E(B-V) Galactic extinction as reported by Schlafly & Finkbeiner (2011).

Columns (17) - IRSF stellar density for stars brighter than 14 mag in K_s band.

[3] If the galaxy is not in the HIZOA catalog 2MASX ID is provided instead.

Table 2: NIR coordinates, sizes, shape and photometry of the brightest 100 galaxies in the catalog in order of isophotal K_{s20} fiducial elliptical aperture magnitude. The full table is available online.

ZOA ID	HI Name	Survey	RA	DEC	l	b	ϵ_J	$r_{K_{s20fe}}$	$J_{K_{s20fe}}$	$H_{K_{s20fe}}$	$K_{sK_{s20fe}}$	μ_{cJ}	μ_{cH}	μ_{cKs}	$E(B-V)$	SD
			(J2000)		[deg]			[arcsec]	[mag]	[mag]	[mag]	[mag arcsec^{-2}]			[mag]	
(1)	(2)	(3)	(4)	(5)	(6)	(7)	(8)	(9)	(10)	(11)	(12)	(13)	(14)	(15)	(16)	(17)
ZOA141309.873-652020.76	J1413-65	HIZOA	213.29114	-65.3391	311.32589	-3.80791	0.44	87.05	7.50 ± 0.02	6.49 ± 0.02	6.09 ± 0.02	12.67	11.69	11.18	1.264	4.374
ZOA151434.147-525921.52	J1514-53	HIZOA	228.64228	-52.98931	323.59395	4.04273	0.77	136.09	8.86 ± 0.02	7.91 ± 0.02	7.42 ± 0.02	14.44	13.49	13.01	0.851	4.299
ZOA085728.473-391605.66	J0857-39	HIZOA	134.36864	-39.26824	261.49959	4.0996	0.10	45.77	9.18 ± 0.02	8.32 ± 0.02	7.95 ± 0.02	14.09	13.22	12.85	0.619	3.611
ZOA150928.962-523320.67	J1509-52	HIZOA	227.37068	-52.55574	323.15549	4.80997	0.79	98.73	9.24 ± 0.02	8.38 ± 0.02	7.97 ± 0.02	14.97	14.05	13.60	0.662	4.090
ZOA081706.065-272720.64	J0817-27	HIZOA	124.27527	-27.45573	246.97346	4.48082	0.41	59.84	9.17 ± 0.02	8.41 ± 0.02	8.11 ± 0.02	14.83	14.09	13.81	0.220	3.746
ZOA181427.987-022505.11	J1814-02	HIZOA	273.61661	-2.41809	26.52553	7.09898	0.47	47.82	10.04 ± 0.02	8.90 ± 0.02	8.50 ± 0.02	14.72	13.70	13.40	1.980	3.986
ZOA122238.290-583657.66	J1222-58	HIZOA	185.65954	-58.61602	299.18024	4.04579	0.69	60.30	9.71 ± 0.02	8.92 ± 0.02	8.60 ± 0.02	14.62	13.83	13.55	0.499	4.121
ZOA151413.880-464827.22	2MASX1514-464	2MASS	228.55783	-46.80756	326.80755	9.33777	0.53	114.03	10.75 ± 0.02	10.16 ± 0.02	8.60 ± 0.02	18.23	17.64	16.89	0.217	3.805
ZOA094916.505-475511.27	J0949-47A	HIZOA	147.31877	-47.9198	274.25667	4.54924	0.10	38.65	9.67 ± 0.02	8.97 ± 0.02	8.69 ± 0.02	14.37	13.62	13.36	0.301	3.797
ZOA145709.815-542331.46	J1457-54	HIZOA	224.2909	-54.39207	320.654	4.09573	0.51	53.80	10.04 ± 0.02	9.14 ± 0.02	8.69 ± 0.02	14.96	14.07	13.64	0.731	4.210
ZOA114606.371-562326.95	J1145-56	HIZOA	176.52655	-56.39082	293.93747	5.33574	0.27	54.68	9.99 ± 0.02	9.26 ± 0.02	8.82 ± 0.02	16.05	15.26	14.82	0.335	3.844
ZOA135138.534-583515.22	J1351-58	HIZOA	207.91056	-58.58756	310.72399	3.3704	0.52	47.27	10.23 ± 0.02	9.31 ± 0.02	8.87 ± 0.02	14.80	13.88	13.41	0.834	4.287
ZOA074752.048-184453.18	J0747-18	HIZOA	116.96687	-18.74811	236.00927	3.37432	0.82	84.90	10.06 ± 0.02	9.31 ± 0.02	8.91 ± 0.02	15.79	14.95	14.77	0.327	3.547
ZOA072210.950-055547.38	J0722-05	HIZOA	110.54563	-5.92983	221.73240	4.08797	0.78	48.64	9.99 ± 0.02	9.28 ± 0.02	8.99 ± 0.02	14.08	13.41	13.05	0.250	3.528
ZOA070103.346+015439.69	J0701+01	HIZOA	105.26394	1.91103	212.32606	3.01075	0.48	41.91	10.16 ± 0.02	9.37 ± 0.02	9.01 ± 0.02	15.09	14.34	13.93	0.520	3.563
ZOA143158.829-552758.82	J1431-55	HIZOA	217.99512	-55.46634	316.91231	4.65254	0.10	34.39	10.32 ± 0.02	9.46 ± 0.02	9.05 ± 0.02	15.65	14.75	14.31	0.731	4.091
ZOA080611.134-273140.86	J0806-27	HIZOA	121.54640	-27.52802	245.70904	2.41392	0.58	43.68	10.26 ± 0.02	9.51 ± 0.02	9.09 ± 0.02	14.84	14.10	13.67	0.420	3.731
ZOA074843.871-261445.62	J0748-26B	HIZOA	117.1828	-26.24601	242.58569	-0.23894	0.32	39.43	10.49 ± 0.02	9.64 ± 0.02	9.10 ± 0.02	15.53	14.56	14.04	0.482	3.723
ZOA163211.878-280530.82	J1632-28	HIZOA	248.04949	-28.0919	351.08364	13.50242	0.72	81.48	10.28 ± 0.02	9.45 ± 0.02	9.10 ± 0.02	15.64	14.80	14.46	0.525	3.536
ZOA141036.181-653457.76	J1410-65	HIZOA	212.65075	-65.58271	310.99728	-3.9582	0.52	46.18	10.35 ± 0.02	9.48 ± 0.02	9.14 ± 0.02	15.13	14.34	13.98	0.516	4.325
ZOA155524.078-581431.30	J1555-581	2MASS	238.85033	-58.24203	325.22158	-3.56961	0.37	65.37	11.32 ± 0.02	9.98 ± 0.02	9.16 ± 0.02	16.32	15.40	14.86	0.641	4.404
ZOA063554.386+110808.32	J0635+11	HIZOA	98.97661	11.13564	201.26237	1.65795	0.27	31.91	10.78 ± 0.02	9.63 ± 0.02	9.19 ± 0.02	15.67	14.70	14.29	1.310	3.518
ZOA083439.531-400855.61	J0834-40	HIZOA	128.66472	-40.14878	259.44805	0.122	0.22	34.38	10.02 ± 0.02	9.52 ± 0.02	9.30 ± 0.02	15.30	14.61	14.51	1.823	3.838
ZOA132723.827-572922.23	J1327-57	HIZOA	201.84928	-57.48951	307.76817	5.04419	0.74	46.73	10.86 ± 0.02	9.82 ± 0.02	9.30 ± 0.02	15.93	14.75	14.09	0.697	3.980
ZOA085838.795-423157.31	J0858-42	HIZOA	134.66165	-42.53259	264.12464	2.14124	0.45	43.00	11.95 ± 0.02	10.10 ± 0.02	9.35 ± 0.02	16.58	14.86	14.05	3.431	3.735
ZOA072456.870-093933.95	J0724-09	HIZOA	111.23696	-9.65943	225.35379	2.94157	0.29	32.86	10.48 ± 0.02	9.71 ± 0.02	9.41 ± 0.02	15.54	14.90	14.39	0.340	3.529
ZOA160349.297-605840.50	2MASX1603-605	2MASS	240.95541	-60.97792	324.23467	-6.33555	0.81	58.98	10.71 ± 0.02	9.85 ± 0.02	9.45 ± 0.02	15.62	15.02	14.67	0.275	4.036
ZOA094952.868-563235.55	J0949-56	HIZOA	147.47029	-56.54321	279.80776	-2.05424	0.24	45.57	11.43 ± 0.02	10.29 ± 0.02	9.58 ± 0.02	16.56	15.33	14.62	1.806	4.159
ZOA141710.092-553240.92	2MASX1417-553	2MASS	214.29205	-55.54470	314.91527	5.31972	0.85	58.28	11.27 ± 0.02	10.13 ± 0.02	9.58 ± 0.02	16.54	15.49	15.10	0.535	3.994
ZOA155422.988-612025.58	2MASX1554-612	2MASS	238.59579	-61.34044	323.13016	-5.86584	0.56	33.80	10.84 ± 0.02	10.11 ± 0.02	9.58 ± 0.02	15.45	15.09	14.44	0.348	4.042
ZOA141933.720-580850.19	J1419-58B	HIZOA	214.8905	-58.14728	314.36294	2.75519	0.59	52.89	11.00 ± 0.02	10.14 ± 0.02	9.59 ± 0.02	16.82	15.82	15.27	1.307	4.363
ZOA163140.118-280606.66	J1631-28	HIZOA	247.91716	-28.10185	350.99666	13.58352	0.27	35.29	10.83 ± 0.02	10.07 ± 0.02	9.59 ± 0.02	15.78	14.94	14.48	0.542	3.598
ZOA161710.946-581845.49	2MASX1617-581	2MASS	244.29561	-58.31264	327.30369	-5.54214	0.57	31.39	10.83 ± 0.02	10.05 ± 0.02	9.61 ± 0.02	15.11	14.33	13.80	0.260	4.203
ZOA101655.552-485252.32	2MASX1016-485	2MASS	154.23147	-48.88120	278.52536	6.52936	0.54	37.76	10.72 ± 0.02	9.74 ± 0.02	9.63 ± 0.02	16.01	15.29	14.91	0.183	3.659
ZOA160425.042-604415.93	2MASX1604-604	2MASS	241.10434	-60.73776	324.45021	-6.20504	0.77	40.77	10.73 ± 0.02	10.01 ± 0.02	9.65 ± 0.02	15.08	14.63	14.42	0.257	4.039
ZOA090033.110-392626.93	J0900-39	HIZOA	135.13796	-39.44081	262.01999	4.43773	0.39	37.83	10.79 ± 0.02	10.15 ± 0.02	9.67 ± 0.02	16.21	15.45	15.04	0.576	3.611
ZOA153603.059-594449.42	2MASXJ1536-5944	2MASS	234.01275	-59.74706	322.32678	-3.22547	0.46	41.50	10.92 ± 0.02	10.04 ± 0.02	9.67 ± 0.02	15.87	14.93	14.40	0.833	4.435
ZOA131033.767-580021.18	J1310-57	HIZOA	197.64070	-58.00588	305.47185	4.77152	0.27	27.20	10.81 ± 0.02	10.02 ± 0.02	9.68 ± 0.02	15.19	14.52	14.22	0.480	4.080
ZOA161319.695-562349.17	J1613-56	HIZOA	243.33207	-56.39699	328.26103	-3.80165	0.35	40.49	10.93 ± 0.02	10.69 ± 0.02	9.68 ± 0.02	16.15	15.39	14.87	0.464	4.425
ZOA074252.007-315959.79	J0742-31	HIZOA	115.7167	-31.99994	246.9317	-4.22566	0.52	26.61	11.15 ± 0.02	10.38 ± 0.02	9.71 ± 0.02	15.39	14.72	14.15	0.714	3.757
ZOA101212.032-623159.40	J1012-62	HIZOA	153.05014	-62.53317	285.68549	-5.12056	0.62	39.84	10.84 ± 0.02	10.08 ± 0.02	9.71 ± 0.02	15.80	15.03	14.51	0.249	4.036
ZOA162101.624-360831.49	J1621-36	HIZOA	245.25677	-36.14208	343.41339	9.76535	0.55	38.44	10.84 ± 0.02	10.05 ± 0.02	9.71 ± 0.02	15.25	14.44	14.09	0.611	3.789
ZOA070056.215-114734.32	J0700-11	HIZOA	105.23423	-11.79287	224.51058	-3.27295	0.70	42.70	11.39 ± 0.02	10.29 ± 0.02	9.72 ± 0.02	16.21	15.12	14.61	0.680	3.595
ZOA072457.474-271516.87	J0724-27	HIZOA	111.23948	-27.25469	240.88167	-5.36564	0.36	41.90	11.78 ± 0.02	11.03 ± 0.02	9.72 ± 0.02	16.64	15.89	15.49	0.370	3.668
ZOA181530.143-025348.41	J1815-02	HIZOA	273.87560	-2.89678	26.22003	6.64723	0.10	32.73	11.41 ± 0.02	10.26 ± 0.02	9.72 ± 0.02	16.32	15.29	14.62	2.230	3.973
ZOA114948.692-640006.93	J1149-64	HIZOA	177.45289	-64.00193	296.24067	-1.9337	0.57	42.66	11.73 ± 0.02	10.42 ± 0.02	9.73 ± 0.02	17.05	15.76	15.05	2.098	4.382
ZOA141710.099-553238.77	J1416-55B	HIZOA	214.29208	-55.5441	314.91548	5.32028	0.86	68.61	11.23 ± 0.02	10.10 ± 0.02	9.73 ± 0.02	16.58	15.47	14.96	0.533	3.982
ZOA074141.201-223112.25	J0741-22	HIZOA	115.42167	-22.52007	238.55754	0.23869	0.80	48.26	11.31 ± 0.02	10.24 ± 0.02	9.74 ± 0.02	16.54	15.35	14.64	0.568	3.737
ZOA161710.749-581844.59	J1617-58	HIZOA	244.29479	-58.31239	327.30356	-5.54166	0.53	33.09	10.82 ± 0.02	10.04 ± 0.02	9.75 ± 0.02	15.19	14.39	14.00	0.258	4.159
ZOA101220.012-471741.58	2MASX1012-471	2MASS	153.08338	-47.29488	276.98315	7.40170	0.81	68.92	11.15 ± 0.02	10.21 ± 0.02	9.76 ± 0.02	16.72	15.89	15.26	0.164	3.478

Continued on Next Page…

Table 2 – Continued

ZOA ID	HI Name	Survey	RA	DEC	l	b	ϵ_J	$r_{K_{s}20fe}$	$J_{K_{s}20fe}$	$H_{K_{s}20fe}$	$K_{sK_{s}20fe}$	μ_{cJ}	μ_{cH}	μ_{cKs}	$E(B-V)$	SD
			(J2000)		[deg]			[arcsec]	[mag]	[mag]	[mag]	[mag arcsec^{-2}]			[mag]	
(1)	(2)	(3)	(4)	(5)	(6)	(7)	(8)	(9)	(10)	(11)	(12)	(13)	(14)	(15)	(16)	(17)
ZOA073008.083-220105.84	J0730-22	HIZOA	112.53368	-22.01829	236.81724	-1.85093	0.77	104.61	11.51 ± 0.02	10.04 ± 0.02	9.79 ± 0.02	17.94	16.76	16.38	1.557	3.695
ZOA075220.625-250840.47	J0752-25A	HIZOA	118.08594	-25.14458	242.05227	1.02238	0.56	33.38	10.92 ± 0.02	10.17 ± 0.02	9.79 ± 0.02	15.47	14.70	14.35	0.327	3.678
ZOA065010.633-111513.52	J0650-11	HIZOA	102.54431	-11.25376	222.83507	-5.38162	0.18	26.46	11.27 ± 0.02	10.36 ± 0.02	9.83 ± 0.02	15.75	14.90	14.42	0.960	3.493
ZOA182226.663-354035.70	J1822-35	HIZOA	275.6111	-35.67658	357.85874	-10.06224	0.65	37.90	10.98 ± 0.02	10.14 ± 0.02	9.84 ± 0.02	16.10	15.22	14.79	0.120	4.113
ZOA164634.204-390308.21	J1646-39	HIZOA	251.64252	-39.05228	344.67632	4.06687	0.24	39.69	11.94 ± 0.02	10.98 ± 0.02	9.85 ± 0.02	16.67	15.79	15.34	0.990	4.446
ZOA141604.868-651502.53	J1416-65	HIZOA	214.02029	-65.2507	311.64365	-3.82057	0.48	36.60	11.23 ± 0.02	10.32 ± 0.02	9.89 ± 0.02	15.77	14.86	14.45	0.662	4.314
ZOA100318.769-645803.19	2MASX1003-645	2MASS	150.82820	-64.96755	286.32177	-7.66814	0.58	29.86	10.93 ± 0.02	9.98 ± 0.02	9.90 ± 0.02	15.68	14.93	14.73	0.197	3.759
ZOA105345.693-625013.17	J1053-62	HIZOA	163.44039	-62.83699	289.95592	-2.96844	0.67	65.48	11.60 ± 0.02	10.68 ± 0.02	9.90 ± 0.02	17.78	16.80	16.23	0.714	4.234
ZOA080708.583-280309.50	J0807-28	HIZOA	121.78576	-28.05264	246.26572	2.31043	0.61	42.80	11.01 ± 0.02	10.29 ± 0.02	9.92 ± 0.02	16.69	16.02	15.56	0.460	3.676
ZOA133732.784-585414.06	J1337-58B	HIZOA	204.3866	-58.90391	308.86656	3.43553	0.28	33.07	11.33 ± 0.02	10.31 ± 0.02	9.92 ± 0.02	16.20	15.11	14.48	0.937	4.303
ZOA143927.759-552503.43	J1439-55	HIZOA	219.86567	-55.41762	317.91041	4.28109	0.22	30.55	11.17 ± 0.02	10.41 ± 0.02	9.97 ± 0.02	16.75	15.92	15.53	0.550	4.110
ZOA105859.839-502155.66	2MASX1058-501	2MASS	164.74933	-50.36546	285.23556	8.60266	0.13	24.61	11.03 ± 0.02	10.11 ± 0.02	9.98 ± 0.02	15.41	14.64	14.33	0.246	3.651
ZOA074901.358-261442.69	J0748-26A	HIZOA	117.25566	-26.24519	242.61809	-0.18219	0.27	26.65	11.49 ± 0.02	10.33 ± 0.02	9.99 ± 0.02	15.56	14.61	14.20	0.619	3.837
ZOA113728.729-644822.59	J1137-644	2MASS	174.36971	-64.80628	295.16228	-3.05609	0.21	26.51	11.96 ± 0.02	10.63 ± 0.02	10.00 ± 0.02	16.35	15.00	14.46	1.363	4.252
ZOA082837.437-371316.76	J0828-37	HIZOA	127.15599	-37.22132	256.39105	0.90411	0.66	36.26	11.42 ± 0.02	10.46 ± 0.02	10.03 ± 0.02	16.18	15.34	14.99	0.920	3.855
ZOA134456.207-654051.40	J1344-65	HIZOA	206.23420	-65.68095	308.40781	-3.37958	0.54	34.10	11.38 ± 0.02	10.47 ± 0.02	10.03 ± 0.02	16.09	15.23	14.68	0.870	4.326
ZOA132159.534-543645.62	2MASX1321-543	2MASS	200.49806	-54.61267	307.39011	7.99438	0.73	41.15	11.28 ± 0.02	10.45 ± 0.02	10.04 ± 0.02	16.63	15.84	15.52	0.349	3.786
ZOA164421.521-552937.33	J1644-55	HIZOA	251.08967	-55.4937	331.91661	-6.33304	0.83	41.24	11.41 ± 0.02	10.41 ± 0.02	10.04 ± 0.02	16.52	15.54	15.03	0.292	4.129
ZOA140835.888-532111.29	2MASX1408-532	2MASS	212.14954	-53.35314	314.41139	7.79011	0.33	33.68	11.00 ± 0.02	10.35 ± 0.02	10.05 ± 0.02	15.50	15.31	15.22	0.424	3.829
ZOA105842.989-501930.65	2MASX1058-501	2MASS	164.67912	-50.32518	285.17723	8.62011	0.82	45.60	11.40 ± 0.02	10.53 ± 0.02	10.08 ± 0.02	16.09	15.27	14.73	0.246	3.651
ZOA064400.636+122407.13	J0644+12	HIZOA	101.00265	12.40198	201.03953	4.00059	0.65	38.29	11.28 ± 0.02	10.55 ± 0.02	10.09 ± 0.02	15.70	15.07	14.46	0.440	3.409
ZOA182423.339-341054.15	J1824-34	HIZOA	276.09725	-34.18171	359.3986	-9.75801	0.36	25.92	11.08 ± 0.02	10.38 ± 0.02	10.09 ± 0.02	15.80	15.05	14.72	0.112	4.079
ZOA154526.828-605931.93	J1545-61	HIZOA	236.36179	-60.99221	322.50754	-4.91839	0.49	27.22	11.49 ± 0.02	10.58 ± 0.02	10.10 ± 0.02	16.00	14.97	14.41	0.611	4.140
ZOA123157.581-595058.07	J1231-595	2MASS	187.98992	-59.84947	300.48507	2.92971	0.28	28.59	11.50 ± 0.02	10.53 ± 0.02	10.11 ± 0.02	16.27	15.32	15.10	0.803	4.215
ZOA151113.653-535743.36	J1511-535	2MASS	227.80689	-53.96205	322.66399	3.46630	0.12	21.61	11.39 ± 0.02	10.52 ± 0.02	10.11 ± 0.02	15.70	15.03	14.87	0.858	4.316
ZOA085809.386-454812.51	J0858-45A	HIZOA	134.53911	-45.80348	266.54398	-0.06235	0.30	28.25	12.14 ± 0.02	10.95 ± 0.02	10.12 ± 0.02	17.26	15.87	15.08	2.356	3.890
ZOA085828.676-451630.99	J0858-45B	HIZOA	134.61948	-45.27528	266.18089	0.32537	0.29	35.29	12.29 ± 0.02	10.94 ± 0.02	10.12 ± 0.02	17.97	16.54	15.77	3.148	3.819
ZOA133724.550-585221.57	J1337-58B	HIZOA	204.35229	-58.87266	308.85465	3.46943	0.68	34.33	11.48 ± 0.02	10.51 ± 0.02	10.12 ± 0.02	15.54	14.67	14.28	0.937	4.303
ZOA154710.889-590408.56	J1547-59	HIZOA	236.79537	-59.06905	323.86792	-3.5382	0.39	47.97	11.32 ± 0.02	10.70 ± 0.02	10.13 ± 0.02	16.82	15.96	15.48	0.550	4.345
ZOA163617.005-421325.00	J1636-421	2MASS	249.07086	-42.22361	340.99750	3.44504	0.39	28.61	11.15 ± 0.02	10.54 ± 0.02	10.13 ± 0.02	16.10	15.30	14.72	1.669	4.401
ZOA165408.098-353438.65	J1653-35	HIZOA	253.53374	-35.57740	348.32502	5.11947	0.13	18.68	11.47 ± 0.02	10.68 ± 0.02	10.17 ± 0.02	15.53	15.12	14.29	0.930	4.395
ZOA140627.300-575142.26	J1406-57	HIZOA	211.61375	-57.86174	312.79903	3.56569	0.27	32.83	11.57 ± 0.02	10.62 ± 0.02	10.18 ± 0.02	16.46	15.50	15.13	0.628	4.171
ZOA160441.177-413947.62	J1604-41	HIZOA	241.17157	-41.66323	337.2209	7.99445	0.35	28.11	11.25 ± 0.02	10.55 ± 0.02	10.18 ± 0.02	16.32	15.53	15.17	0.559	3.887
ZOA090240.287-413502.67	J0902-413	2MASS	135.66787	-41.58408	263.90158	3.32788	0.52	28.06	11.53 ± 0.02	10.61 ± 0.02	10.19 ± 0.02	16.09	15.18	14.80	1.000	3.659
ZOA155335.142-614059.08	2MASX1553-614	2MASS	238.39643	-61.68308	322.83628	-6.06836	0.74	38.79	11.32 ± 0.02	10.51 ± 0.02	10.20 ± 0.02	16.10	15.50	15.47	0.287	4.020
ZOA182700.997-203159.00	J1826-20	HIZOA	276.75416	-20.53306	11.92447	-4.08824	0.70	41.25	11.59 ± 0.02	10.62 ± 0.02	10.20 ± 0.02	16.62	15.62	15.17	0.714	4.688
ZOA140621.248-602544.76	J1406-602	2MASS	211.58854	-60.42910	312.05114	1.10944	0.42	22.18	12.47 ± 0.02	10.97 ± 0.02	10.21 ± 0.02	16.55	15.26	14.53	2.962	4.638
ZOA134423.990-522211.32	2MASX1344-522	2MASS	206.09996	-52.36981	311.08708	9.66132	0.75	40.16	11.57 ± 0.02	10.64 ± 0.02	10.22 ± 0.02	16.65	15.79	15.43	0.387	3.632
ZOA170643.848-482357.97	2MASXJ1706-4823	2MASS	256.68270	-48.39944	339.64225	-4.60656	0.71	28.00	11.68 ± 0.02	10.79 ± 0.02	10.24 ± 0.02	16.10	15.27	14.60	0.747	4.363
ZOA080953.826-414136.58	J0809-41	HIZOA	122.47428	-41.69349	258.04937	-4.6003	0.84	66.41	12.03 ± 0.02	10.82 ± 0.02	10.25 ± 0.02	17.66	16.41	15.72	1.049	3.750
ZOA151548.734-600409.37	J1515-60B	HIZOA	228.95306	-60.06927	320.0373	-2.08271	0.17	32.38	12.09 ± 0.02	10.84 ± 0.02	10.25 ± 0.02	17.56	16.25	15.61	3.113	4.611
ZOA165805.966-211622.32	J1658-21A	HIZOA	254.52486	-21.27287	0.33099	13.19049	0.12	28.09	11.30 ± 0.02	10.52 ± 0.02	10.27 ± 0.02	16.21	15.52	15.39	0.300	3.667
ZOA105838.725-645044.49	J1058-645	HIZOA	164.66136	-64.84569	291.30815	-4.55072	0.16	22.02	11.53 ± 0.02	10.65 ± 0.02	10.28 ± 0.02	15.82	14.93	14.84	0.533	4.122
ZOA160449.497-414301.20	J1604-41	HIZOA	241.20624	-41.717	337.20382	7.93721	0.44	36.21	11.42 ± 0.02	10.71 ± 0.02	10.29 ± 0.02	16.40	15.62	15.24	0.559	3.887
ZOA183155.989-314742.59	J1831-31	HIZOA	277.98329	-31.79516	2.28022	-10.13403	0.35	32.63	11.24 ± 0.02	10.57 ± 0.02	10.30 ± 0.02	16.16	15.49	15.21	0.146	4.054
ZOA063556.737+143557.75	J0635+14B	HIZOA	98.98641	14.59938	198.18527	3.25387	0.20	21.72	11.49 ± 0.02	10.66 ± 0.02	10.31 ± 0.02	15.74	14.92	14.65	0.570	3.529
ZOA120920.790-622912.31	J1209-62	HIZOA	182.33663	-62.48676	298.09238	-0.01117	0.36	22.97	13.08 ± 0.02	11.21 ± 0.02	10.31 ± 0.02	17.35	15.59	14.70	3.294	4.553
ZOA141232.785-563433.93	J1412-56A	HIZOA	213.13661	-56.57609	313.97218	4.54707	0.46	42.52	11.43 ± 0.02	10.62 ± 0.02	10.32 ± 0.02	17.21	16.41	16.07	0.559	4.149
ZOA072653.624-073252.01	J0726-07	HIZOA	111.72344	-7.54778	223.71538	4.36180	0.21	27.41	11.00 ± 0.02	10.64 ± 0.02	10.35 ± 0.02	16.59	16.08	15.80	0.240	3.492
ZOA100655.897-450248.59	2MASX1006-450	2MASS	151.73290	-45.04683	274.89188	8.68243	0.65	33.97	11.43 ± 0.02	10.72 ± 0.02	10.35 ± 0.02	16.53	15.93	15.52	0.132	3.504

Table 3. Summary of the characteristic properties of the catalog.

Parameter	Mean	Max.	Min.
ϵ_J	0.42	0.90	0.10
$r_{K_{s20fe}}$ [arcsec]	15.57	136.08	0.51
$J_{K_{s20fe}}$ [mag]	14.28	22.08	7.50
$H_{K_{s20fe}}$ [mag]	13.39	22.65	6.49
$K_{sK_{s20fe}}$ [mag]	13.02	23.02	6.09
$E(B-V)$ [mag]	0.92	12.76	0.09
SD	3.95	5.32	3.28

4.2 Data presentation

Table 3 and Figure 5 summarize the characteristic properties of the NIR catalog. In Table 3 we list the mean, maximum and minimum for a number of parameters. These parameters are as follows:

- (ϵ_J) J-band ellipticity
- ($r_{K_{s20fe}}$) K_{s20} fiducial elliptical aperture semi-major axis
- ($J_{K_{s20fe}}$, $H_{K_{s20fe}}$, and $K_{sK_{s20fe}}$) J, H, and K_s bands K_{s20} fiducial elliptical aperture magnitudes
- ($E(B-V)$) Galactic extinction as reported by Schlafly & Finkbeiner (2011)
- (SD) IRSF stellar density for stars brighter than 14 mag in K_s band.

Figure 5 shows histograms of all parameters except $E(B-V)$ and stellar density which are discussed in detail in the next section as part of the completeness. The top panels, a and b, in Fig. 5 show the distribution of the shape and size of 1044 galaxies in the catalog. The bottom panels, c, d, and e, show the distribution of the photometric parameters in J, H, and K_s bands, respectively.

Panel A shows that our sample contains a fairly flat distribution which is consistent with expectation of a random sample of disk galaxies. However, for our final TF sample we use only edge-on galaxies after applying the axial ratio correction from Said et al. (2015). In panel b we plot a histogram of the distribution of the K_{s20} fiducial elliptical aperture semi-major axis. Panel b shows that only three galaxies in our sample have $r_{K_{s20fe}}$ larger than 100 arcsec and 21 galaxies are larger than 50 arcsec. The largest three galaxies are J1514-53, 2MASX1514-464, and J0730-22 which have $r_{K_{s20fe}}$ of 136, 114 and 104 arcsec, respectively.

In panels c, d, and E we show histograms of the distribution of J, H, and K_s bands K_{s20} fiducial elliptical aperture magnitudes. The deep NIR survey of the Norma Wall (Riad 2010; Kraan-Korteweg et al. 2011), which used the same IRSF instrument with the same setup, found that the completeness limit is $J^\circ = 15.6$, $H^\circ = 15.3$, and $K_s^\circ = 14.8$ mag in J, H, and K_s band, respectively. However, these limits are only valid for $A_{K_s} < 1.0$ mag and $\log(N_{(K_s<14)}/deg^2) < 4.71$. Compared to other NIR surveys, the IRSF survey is 1 mag deeper than 2MASS in the J band and 2.0 mag deeper in the K_s band. However, it is only one magnitude shallower than the UKIDSS Galactic Plane Survey (GPS; Lucas et al. 2008) and VISTA Variables in the Via Lactea (VVV; Amôres et al. 2012) in the K_s band. In Section 6.3 we run a full comparison with UKIDSS GPS galaxies. The three panels (c, d, and e) of Fig. 5 show that the detection rate drops rapidly for galaxies fainter than 16 mag. However, this survey is not a magnitude limited in any sense. Panel E shows that our survey has 63 galaxies brighter than 10 mag.

5 COMPLETENESS

In this section we discuss the completeness as a function of dust extinction, stellar density and H I mass. We divided the catalog into three sub-samples as a function of their logarithm H I mass reported in Staveley-Smith et al. (2016). The first column in Fig. 6 shows galaxies with $\log M_{HI}[M_\odot] \geqslant 9.5$. The second column presents galaxies within the range of $8.5 \leqslant \log M_{HI}[M_\odot] < 9.5$. The third column shows any galaxy with $\log M_{HI}[M_\odot] < 8.5$.

The top panels in Fig. 6 show the completeness as a function of the IRSF stellar density for stars brighter than 14 mag in the K_s band for the three sub-samples. The first two columns in the top panel show that detection rate is 100% of massive galaxies ($\log M_{HI}[M_\odot] > 8.5$) in regions with stellar density of $\log(N_{K_s<14}/deg^2) \leqslant 4$. This detection rate can drop to 50% for regions within $4 < \log(N_{K_s<14}/deg^2)$. However, the third column in the top panel shows that the detection rate of the less massive galaxies ($\log M_{HI}[M_\odot] < 8.5$) is 75% complete in regions of $\log(N_{K_s<14}/deg^2) \leqslant 4$ and only 30% in regions with stellar density of $4 < \log(N_{K_s<14}/deg^2)$.

Similar conclusion can be made from the bottom panels of Fig. 6 which show the completeness as a function of Galactic reddening along the line of sight (Schlafly & Finkbeiner 2011). The first two columns in the bottom panel show the detection of the massive galaxies which is nearly 90% for galaxies in regions of $E(B-V) \leqslant 1$ mag ($A_V = 3.1$ mag). Furthermore, we still can detect massive galaxies up to $E(B-V) = 7$ mag ($A_V = 21.7$ mag). On the contrary, the third column in the bottom panel shows that the detection of less massive galaxies is not complete even in regions with $E(B-V) \leqslant 1$ mag ($A_V = 3.1$ mag).

6 COUNTERPARTS AND COMPARISONS

In this section we discuss the counterparts of our survey. We present the confirmed HIZOA counterparts then check for counterparts in the 2MASX (Jarrett et al. 2000) and UKIDSS GPS (Lucas et al. 2008) surveys.

6.1 HIZOA counterparts

The pixel size of the final HIZOA cubes of 4 arcmin in RA and DEC makes the IRSF instrument perfect for the follow up observations given the 8.6×8.6 arcmin^2 field of view (after dithering). This means that, for each pointing we should find at least one H I source. Thus, the detection of these H I sources depends on their H I mass and the stellar density and dust extinction of the region they lie in. Some NIR fields have more than one source and need more attention. All sources identified as H I sources in the NIR fields are inspected by eye and compared with the H I profiles. A galaxy with double-horn H I profile was normally identified as an edge-on galaxy in the NIR image. However, a galaxy with a Gaussian profile was usually identified with face-on galaxy in the NIR image. The color of the galaxy in the NIR image was also used.

The final NIR catalog contains 684 confirmed counterpart galaxies in the three HIZOA catalogs (HIZOA-S; Staveley-Smith et al. 2016, HIZOA-N; Donley et al. 2005, GB; Kraan-Korteweg et al. 2008).

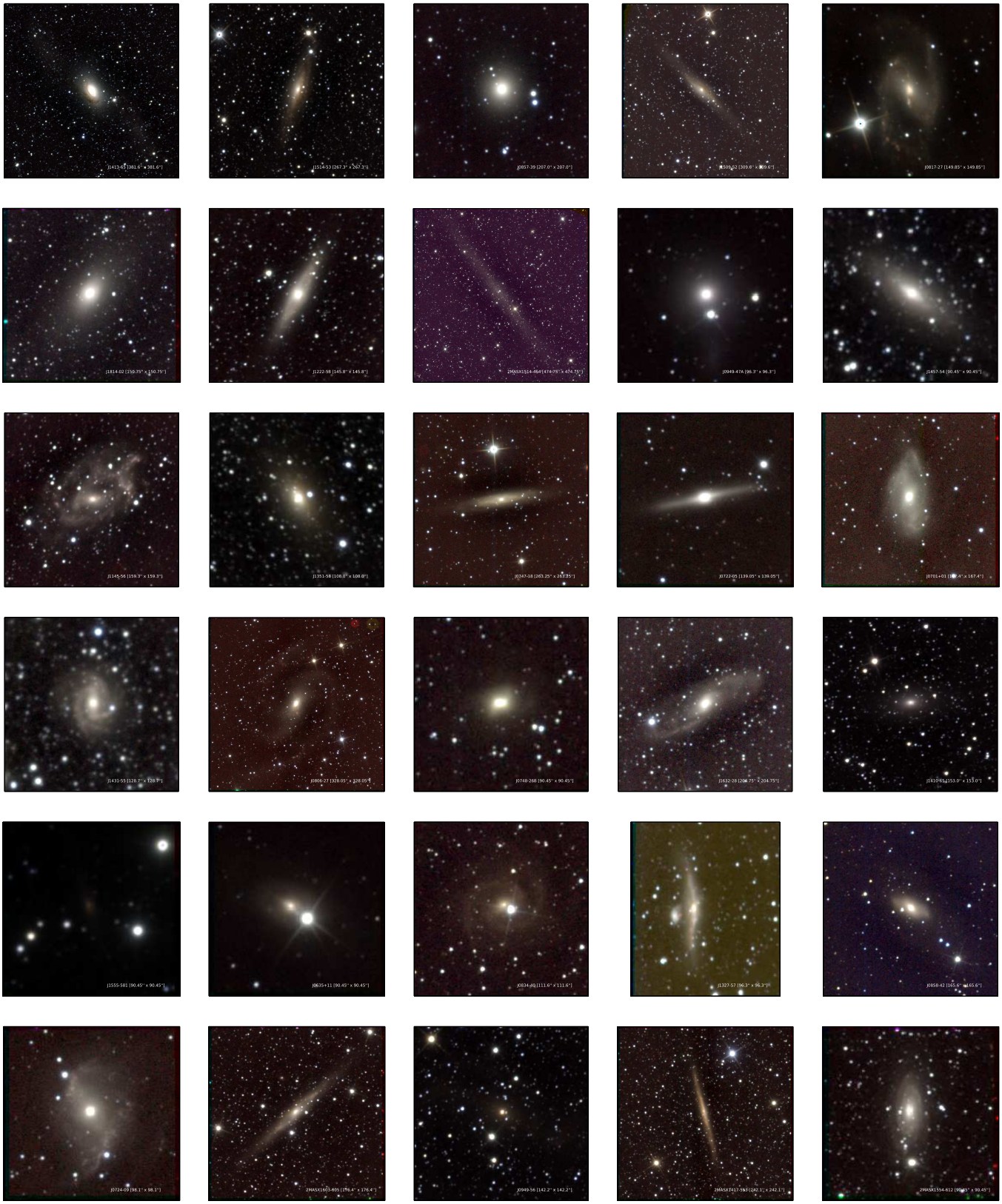

Figure 4. Postage stamp images of the brightest 100 galaxies in the catalog in order of isophotal K_{s20} fiducial elliptical aperture magnitude. The color composite is derived in the standard fashion: blue J band, green H band, and red K_s band.

Figure 4. Continued

Figure 4. Continued

Figure 4. Continued

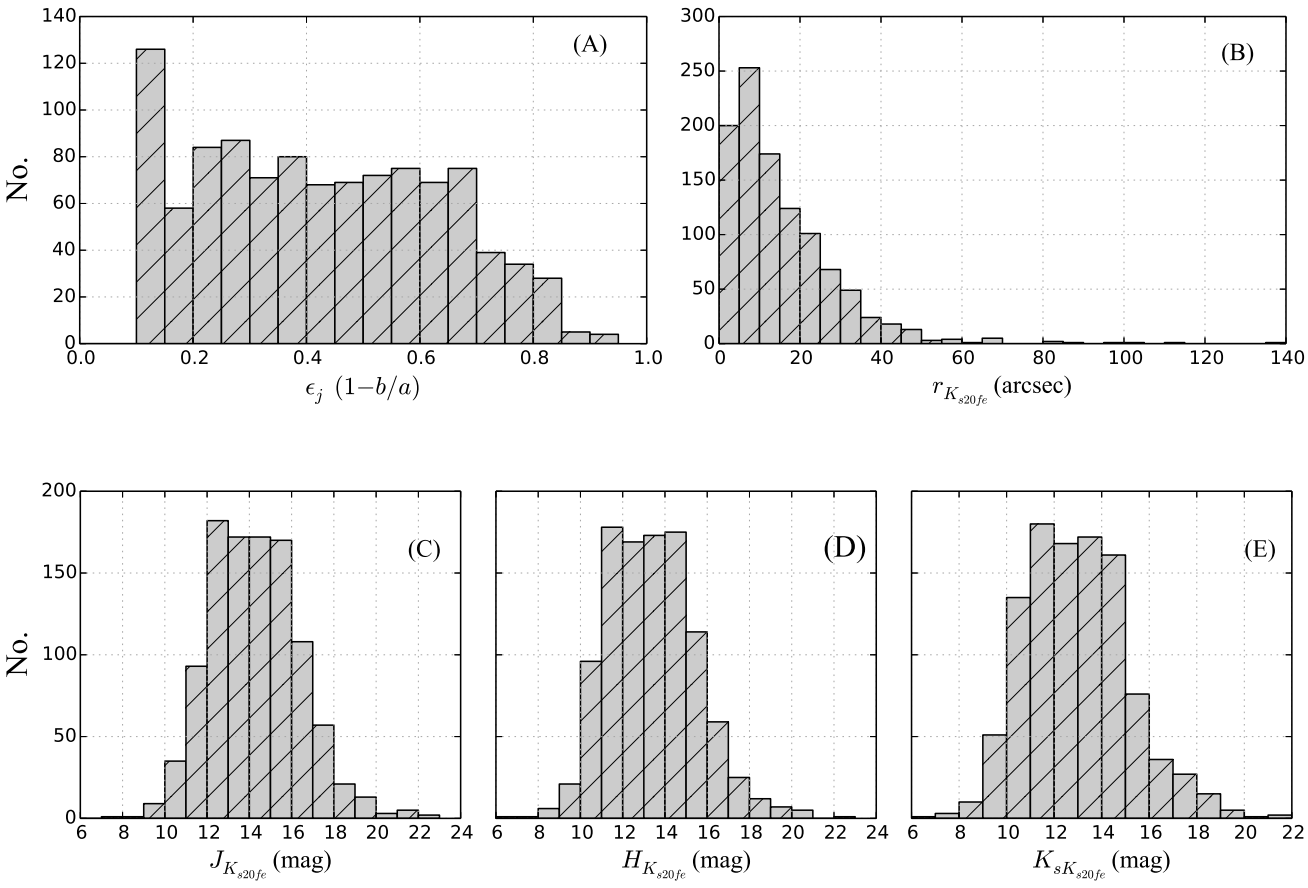

Figure 5. Summary of the characteristic photometric properties of the catalog. The top panels A and B show the distribution of the shape, represented by (ϵ_J) the J-band ellipticity, and size, represented by $(r_{K_{s20fe}})$ K_{s20} fiducial elliptical aperture semi-major axis, of 1044 galaxies in the catalog. The bottom panels C, D, and E show the distribution of the photometry represented by K_{s20} fiducial elliptical aperture magnitudes in J, H, and K_s bands, respectively.

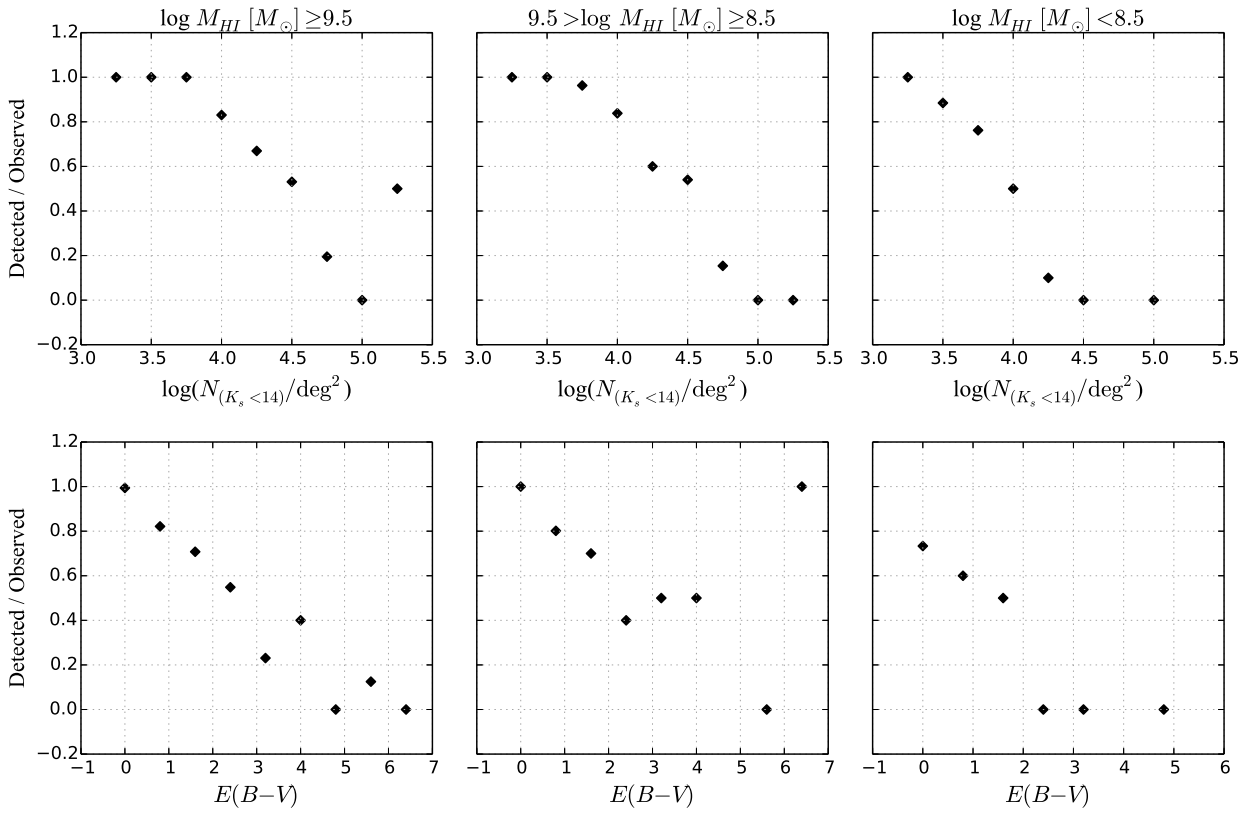

Figure 6. The completeness as a function of dust, stellar density and HI mass. The three columns present the whole catalog divided into three sub-samples as a function of HI mass. The top panels show the completeness as a function of log of the stellar density for stars brighter than 14 mag in the K_s band. The bottom panels show the completeness as a function of Galactic reddening along the line of sight.

6.2 2MASS counterparts

Of the NIR 1044 galaxies in the final catalog, 285 have counterparts in the 2MASX catalog. We used a search radius of only 1 arcsec because of the high positional accuracy of both 2MASS and IRSF. In Fig. 7 we compare our derived K_s bands K_{s20} fiducial elliptical aperture magnitudes with the same parameter in the 2MASX catalog (Jarrett et al. 2000, 2003) for these 285 galaxies.

Figure 7 shows good agreement between the K_{s20} derived for this catalog and the same parameter reported in the 2MASX catalog. Small systematic deviations, < 0.8 mag, are shown for both faint galaxies (> 14 mag) marked as blue circles and bright galaxies (< 9 mag) marked as red circles. This deviation is due to the difference of the pixel scale between these two instruments. IRSF has pixel scale of 0.45 arcsec pixel^{-1} compared to 2.0 arcsec pixel^{-1} for the 2MASX survey. Top-panels of sub-figures (b) and (c) show that small-faint stars superimposed on the galaxy can not be resolved by 2MASX. Thus, the magnitude of this galaxy is over-estimated because these stars are not subtracted from the image before running the photometry process. The high resolution of the IRSF instrument as shown on the bottom panels of sub-figures (b) and (c), lead to a more effective star-subtraction process and thus more accurate photometry which is vital for working in the ZOA.

6.3 UKIDSS counterparts

The UKIDSS Galactic Plane Survey (GPS) (Lucas et al. 2008) overlaps with the HIZOA survey in the Northern extension published in the Donley et al. (2005). We used the *UKIDSS DR8 plus* data release which is the GPS publically accessible to search for counterparts. Given the high position accuracy of both IRSF and UKIDSS GPS, the minimum search radius available online of 3 arcsec was used. We found 30 confirmed counterparts in the UKIDSS GPS survey. A modified version of our IRSF photmetry-pipeline was used to derive the photometric parameters for these UKIDSS GPS images.

Figure 8 shows the comparison between K_s bands K_{s20} fiducial elliptical aperture magnitudes derived from the IRSF images and the same parameter derived from the UKIDSS GPS images. The solid line in Fig. 8 is the one-to-one line. A perfect agreement between IRSF and UKIDSS GPS can be seen. The pixel scale for the UKIDSS GPS images are 0.4 arcsec pixel^{-1} which is comparable to the IRSF pixel scale of 0.45 arcsec pixel^{-1}. This led to a similar average seeing of 1.54 arcsec for the UKIDSS GPS images used in this comparison and 1.38 arcsec of the IRSF survey. This agreement shows that the IRSF imaging is not suffering from foreground contamination, after star removal, nor is it adversely under-estimating the isophotal flux of the ZOA galaxies.

The UKIDSS GPS survey will be used to extend the TF project in the Northern ZOA along with the H I data from the Nançay Radio Telescope.

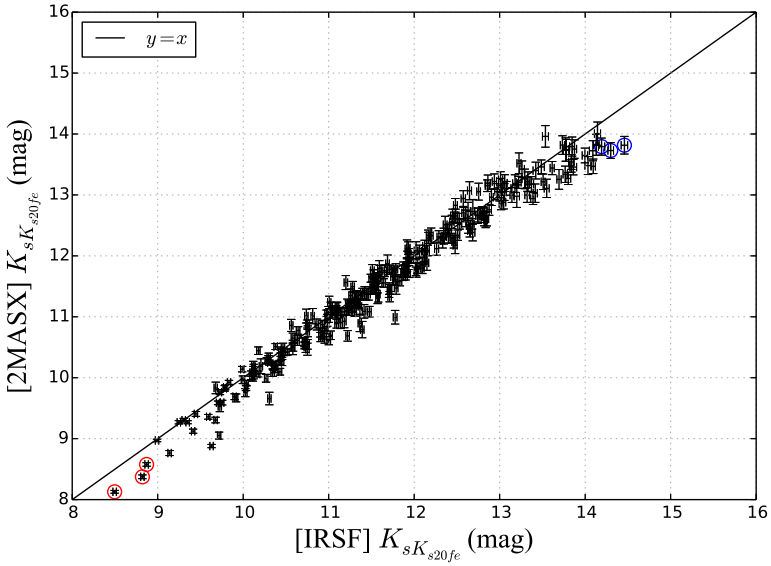

(a) one-to-one Comparison

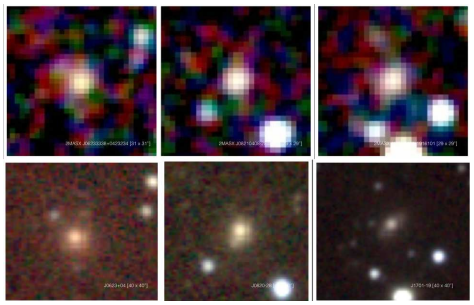

(b) Faintest galaxies marked by blue circles

(c) Brightest galaxies marked by blue circles

Figure 7. A Comparison between K_s bands K_{s20} fiducial elliptical aperture magnitudes derived for this catalog and the same parameter reported in the 2MASX catalog. (a) one-to-one comparison; the solid line shows the one-to-one relation. (b) Postal stamps of the faintest three galaxies marked as blue circles; top panels are 2MASX and bottom panels are the IRSF. (c) The brightest three galaxies marked as red circles; top panels are 2MASX and bottom panels are the IRSF. Name and size of each image is printed on the bottom-right corner of each stamp.

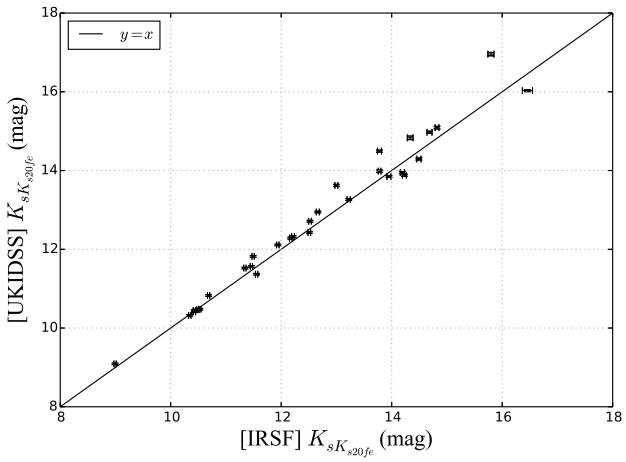

Figure 8. A comparison between K_s bands K_{s20} fiducial elliptical aperture magnitudes derived from the IRSF images and the same parameter derived from the UKIDSS GPS images using a modified version of the IRSF photometry-pipeline to fit the UKIDSS images. The solid line is the one-to-one line. The dashed line is the best fit line.

7 SUMMARY

In this paper, we present the observations, data reduction and final catalog for 1229 NIR fields, in the J, H, and K_S bands, in the southern Zone of Avoidance. The observations were conducted between 2006 and 2013 using the Infrared Survey Facility (IRSF) installed on the 1.4 m telescope situated at the South African Astronomical Observatory site in Sutherland. This resulted in observations of all galaxies in the three blind systematic deep H I ZOA surveys (Donley et al. 2005; Kraan-Korteweg et al. 2008; Staveley-Smith et al. 2016). The final catalog contains 1044 NIR galaxies in the J, H, and K_S bands.

The quality of the images is discussed in detail. The survey has an average seeing and zero point magnitude of 1.38 arcsec and 20.1 mag in the K_s band. These values agrees with previous surveys done with the same instrument.

The completeness as a function of stellar density and dust extinction was found to be dependent on the H I mass of each galaxy.

Using our method of matching, we identified 684 galaxies in the final NIR catalog that have confirmed counterparts in the three HIZOA catalogs. Counterparts from similar NIR surveys are presented. We found 285 2MASX galaxies have counterparts in our final catalog. However, only 30 galaxies in the UKIDSS Galactic Plane Survey have counterparts in our final NIR catalog because UKIDSS GPS overlap with our survey only in its northern extension.

We found good agreement between the K_s band K_{s20} fiducial elliptical aperture magnitude derived in this paper and the same parameter reported in the 2MASX catalog. We detect only small deviations in K_{s20} of < 0.8 mag for both faint galaxies (> 14 mag) and bright galaxies (< 9 mag). This is due to the difference of the pixel scale between IRSF and 2MASX instruments. IRSF has pixel scale of 0.45 arcsec pixel^{-1} compared to 2.0 arcsec pixel^{-1} for the 2MASX survey.

Good agreement between the K_s band K_{s20} fiducial elliptical aperture magnitude derived from the IRSF data and the UKIDSS GPS data was also shown. This agreement shows that the IRSF

imaging is as good as the UKIDSS GPS images which is one magnitude deeper. This also means that IRSF images is neither suffering from foreground contamination, after star removal, nor is it under-estimating the isophotal flux of the ZOA galaxies. The derivation of UKIDSS parameters is regarded as a pilot project of our TF survey in the northern ZOA.

This paper is the third component of our TF survey. The data presented here will be used with the recently calibrated TF relation in Said et al. (2015) as well as the H I data presented in Said et al. (2016) to derive distances and peculiar velocities for inclined spiral galaxies in the southern ZOA. Extension of this project into the northern ZOA already started last year with the H I observations of bright inclined 2MASS galaxies using the Nançay Radio Telescope.

ACKNOWLEDGMENTS

This work is based upon research supported by the Science Faculty at University of Cape Town (UCT), the South African National Research Foundation and the Department of Science and Technology. Part of this research was conducted by the Australian Research Council Centre of Excellence for All-sky Astrophysics (CAASTRO), through project number CE110001020. We thank Dr. Tom Mutabazi and Hiroki Onozato for running some of the observations. We also thank Dr. Yasushi Nakajima, Dr. Takahiro Nagayama and Dr. Ihab Riad for many discussions regarding the reduction pipeline. The authors are very grateful to Dr. Christina Magoulas for her careful reading and comments on the paper.

REFERENCES

Amôres E. B. et al., 2012, AJ , 144, 127
Carrick J., Turnbull S. J., Lavaux G., Hudson M. J., 2015, MNRAS , 450, 317
Courtois H. M., Pomarède D., Tully R. B., Hoffman Y., Courtois D., 2013, AJ , 146, 69
Cutri R. M. et al., 2003, 2MASS All Sky Catalog of point sources.
Donley J. L. et al., 2005, AJ , 129, 220
Dressler A., Faber S. M., Burstein D., Davies R. L., Lynden-Bell D., Terlevich R. J., Wegner G., 1987, ApJL , 313, L37
Einasto J., Joeveer M., Saar E., 1980, MNRAS , 193, 353
Focardi P., Marano B., Vettolani G., 1984, A&A, 136, 178
Giovanelli R., Haynes M. P., 1982, AJ , 87, 1355
Hauschildt M., 1987, A&A, 184, 43
Hong T. et al., 2014, MNRAS , 445, 402
Hong T. et al., 2013, MNRAS , 432, 1178
Jarrett T.-H., Chester T., Cutri R., Schneider S., Rosenberg J., Huchra J. P., Mader J., 2000, AJ , 120, 298
Jarrett T. H., Chester T., Cutri R., Schneider S., Skrutskie M., Huchra J. P., 2000, AJ , 119, 2498
Jarrett T. H., Chester T., Cutri R., Schneider S. E., Huchra J. P., 2003, AJ , 125, 525
Jarrett T. H. et al., 2007, AJ , 133, 979
Kraan-Korteweg R. C., 2005, in Röser S., ed., Reviews in Modern Astronomy Vol. 18, Reviews in Modern Astronomy. pp 48–75
Kraan-Korteweg R. C., Lahav O., 2000, A&A Rev., 10, 211
Kraan-Korteweg R. C., Riad I. F., Woudt P. A., Nagayama T., Wakamatsu K., 2011, ArXiv e-prints
Kraan-Korteweg R. C., Shafi N., Koribalski B. S., Staveley-Smith L., Buckland P., Henning P. A., Fairall A. P., 2008, Outlining the Local Void with the Parkes HI ZOA and Galactic Bulge Surveys. p. 13
Lagattuta D. J., Mould J. R., Staveley-Smith L., Hong T., Springob C. M., Masters K. L., Koribalski B. S., Jones D. H., 2013, ApJ , 771, 88
Lucas P. W. et al., 2008, MNRAS , 391, 136
Lynden-Bell D., Faber S. M., Burstein D., Davies R. L., Dressler A., Terlevich R. J., Wegner G., 1988, ApJ , 326, 19
Magoulas C. et al., 2012, MNRAS , 427, 245
Masters K. L., Springob C. M., Haynes M. P., Giovanelli R., 2006, ApJ , 653, 861
Masters K. L., Springob C. M., Huchra J. P., 2008, AJ , 135, 1738
Mutabazi T., Blyth S. L., Woudt P. A., Lucey J. R., Jarrett T. H., Bilicki M., Schröder A. C., Moore S. A. W., 2014, MNRAS , 439, 3666
Nagayama T. et al., 2003, in Iye M., Moorwood A. F. M., eds, Proc. SPIEVol. 4841, Instrument Design and Performance for Optical/Infrared Ground-based Telescopes. pp 459–464
Nagayama T. et al., 2004, MNRAS , 354, 980
Nagayama T. et al., 2006, MNRAS , 368, 534
Neill J. D., Seibert M., Tully R. B., Courtois H., Sorce J. G., Jarrett T. H., Scowcroft V., Masci F. J., 2014, ApJ , 792, 129
Riad I. F., 2010, PhD thesis, , Univ. of Cape Town, South Africa, (2010)
Riad I. F., Kraan-Korteweg R. C., Woudt P. A., 2010, MNRAS , 401, 924
Said K., Kraan-Korteweg R. C., Jarrett T. H., 2015, MNRAS , 447, 1618
Said K., Kraan-Korteweg R. C., Staveley-Smith L., Williams W. L., Jarrett T. H., Springob C. M., 2016, MNRAS , 457, 2366
Schlafly E. F., Finkbeiner D. P., 2011, ApJ , 737, 103
Skrutskie M. F. et al., 2006, AJ , 131, 1163
Sorce J. G. et al., 2013, ApJ , 765, 94
Sorce J. G., Tully R. B., Courtois H. M., Jarrett T. H., Neill J. D., Shaya E. J., 2014, MNRAS , 444, 527
Springob C. M. et al., 2016, MNRAS , 456, 1886
Springob C. M. et al., 2014, MNRAS , 445, 2677
Springob C. M., Masters K. L., Haynes M. P., Giovanelli R., Marinoni C., 2007, ApJS , 172, 599
Staveley-Smith L., Kraan-Korteweg R. C., Schröder A. C., Henning P. A., Koribalski B. S., Stewart I. M., Heald G., 2016, AJ , 151, 52
Tully R. B., Courtois H., Hoffman Y., Pomarède D., 2014, Nature , 513, 71
Tully R. B., Courtois H. M., Sorce J. G., 2016, ArXiv e-prints
Tully R. B., Fisher J. R., 1987, Atlas of Nearby Galaxies
Williams W. L., Kraan-Korteweg R. C., Woudt P. A., 2014, MNRAS , 443, 41
Woudt P. A., Fairall A., Kraan-Korteweg R. C., Lucey J., Schröder A., Burstein D., McCall M. L., 2005, in Fairall A. P., Woudt P. A., eds, Astronomical Society of the Pacific Conference Series Vol. 329, Nearby Large-Scale Structures and the Zone of Avoidance. p. Fairall
Woudt P. A., Kraan-Korteweg R. C., Fairall A. P., 1999, A&A, 352, 39

This paper has been typeset from a TEX/ LATEX file prepared by the author.